Available online at www.sciencedirect.com
SCIENCE DIRECT®
Journal of Solid State Chemistry 177 (2004) 3595–3602
JOURNAL OF SOLID STATE CHEMISTRY
http://elsevier.com/locate/jssc

Crystal structure and vibrational properties of nonlinear Eu_3BWO_9 and Nd_3BWO_9 crystals

M. Mączka,[a,*] P. Tomaszewski,[a] J. Stępień-Damm,[a] A. Majchrowski,[b] L. Macalik,[a] and J. Hanuza[a,c]

[a] *Institute of Low Temperature and Structure Research, Polish Academy of Sciences, ul. Okolna 2, P.O. Box 1410, 50-950 Wrocław 2, Poland*
[b] *Institute of Applied Physics, Military University of Technology, 2 Kaliskiego Str., 00-908 Warszawa, Poland*
[c] *Department of Bioorganic Chemistry, Faculty of Industry and Economics, University of Economics, ul. Komandorska 118/120, 53-345 Wrocław, Poland*

Received 27 January 2004; received in revised form 16 April 2004; accepted 2 June 2004

Available online 12 August 2004

Abstract

IR, Raman, X-ray, electron absorption and luminescence studies have been performed for novel laser Nd_3BWO_9 and Eu_3BWO_9 borotungstates exhibiting non-centrosymmetric crystal structures. The assignment of observed vibrational modes to respective symmetry and vibrations of atoms has been proposed. These studies have shown that vibrational and electronic properties of these crystals can be better explained when $P6_3$ symmetry is assumed, instead of previously proposed $P3$ one. The crystal structure refinement has also confirmed that symmetry of the Eu_3BWO_9 borotungstates is $P6_3$, not $P3$.

Keywords: Phonon properties; Electronic transitions; Crystal structure

1. Introduction

Complex boron oxide compounds attract considerable attention because they can be used as multifunctional optical materials in which the laser effect and nonlinear optical phenomena occur simultaneously. One of the promising group of complex boron oxides are borotungstates with the general formula Ln_3BWO_9, where Ln = La, Pr, Nd, Sm–Ho. It was shown previously that these compounds exhibit second harmonic generation [1]. The SHG magnitude was 3–25 times larger than that of quartz, depending on the lanthanide ion [1]. The crystal structure was found to be closely related to the centrosymmetric $P6_3/m$ structure of $Ln_3WO_6Cl_3$ compounds [2,3]. However, the boron cations are displaced from the mirror plane and the WO_6 polyhedra are distorted resulting either in $P6_3$ structure (for La) or $P3$ structure (for Pr–Ho) [2,3]. It has been suggested that the increased optical nonlinearity with increasing Ln atomic mass is due to increased distortion of the WO_6 polyhedra [1].

The purpose of the present paper is to give insight into lattice dynamics of this promising but insufficiently studied group of compounds. Our Raman and IR studies showed that there exist very significant discrepancies between the observed spectra and predicted selection rules based on the $P3$ symmetry. In particular, these results suggested that there is only one crystallographically distinct BO_3^{3-} and WO_6 group, whereas two distinct sites occupied by BO_3^{3-}, WO_6 and lanthanide ions should be present in the $P3$ structure. In order to obtain some additional information on the borotungste structure, we decided to perform additional electron absorption and luminescence studies of europium compound. This study has shown very clearly that there is only one site occupied by the Eu^{3+} ions. The presence of single sites occupied by BO_3^{3-}, WO_6 and Eu^{3+} ions provide a very strong indication that the $P3$ structure, suggested on the basis of X-ray studies [2], is not correct and that the structure may be the same as found for the lanthanum derivative, i.e., $P6_3$. Our

*Corresponding author. Fax: +48713441029.
E-mail address: maczka@int.pan.wroc.pl (M. Mączka).

0022-4596/$ - see front matter © 2004 Elsevier Inc. All rights reserved.
doi:10.1016/j.jssc.2004.06.016

present X-ray study of the Eu_3BWO_9 crystal supports this conclusion.

2. Experiment

For the first time description of rare-earth borotungstates crystallization was given by Gokhman et al. [2]. Spontaneous crystallization from molten PbO was carried out in the 1100–800°C range at a cooling rate 4–6°C/h. The molar compositions of fluxes for rare-earth borotungstates (RE = La, Pr, Nd, Sm–Ho) single crystal growth were also given in Ref. [2]. According to the Nd_2O_3:B_2O_3:WO_3 phase diagram given by Dzhurinskii et al. [3] three ternary compounds can be formed: Nd_3BWO_9, $Nd_2B_2WO_9$, and $Nd(BO_2)WO_4$. Moreover several double compounds, like $Nd_4W_9O_{33}$, can also be formed. In case of neodymium borotungstate crystallization, to avoid the formation of phases enriched in tungsten or boron ions, what might be promoted by high molar content of WO_3 in case of the composition used by Gokhman et al. [2], we used almost stoichiometric molar composition of Nd_3BWO_9 constituents 3:1.1:2.2 (Nd_2O_3:B_2O_3:WO_3) [4]. The concentration of neodymium borotungstate in PbO was equal to 15 mol%. In case of europium borotungstate we used starting compositions given in Ref. [2]. Crystallization was carried out in a platinum crucible covered with a lid. A resistance furnace with precise temperature control (Eurotherm 906S programmer) allowed to change the temperature linearly at rates from 0.1 to 100°C/h range. The soaking temperature was 1100°C, similarly to Gokhman work, but the cooling rates were much lower—0.3–0.5°C/h instead of 4–6°C/h. After the solidification of the melt the furnace was cooled down to the room temperature at a rate 20°C/h, and then borotungstate crystals were extracted from the crucible by means of etching in hot alkaline solution. Borotungstate single crystals were grown in form of hexagonal rods up to 5 mm in length and up to $2 \times 2\,mm^2$ in cross-section for neodymium and up to 2 mm in length and $0.3 \times 0.3\,mm^2$ in cross-section for europium.

Polycrystalline infrared spectra were measured with a Biorad 575C FT-IR spectrometer as KBr pellets in the 1500–400 cm^{-1} region and in Nujol suspension for the 500–30 cm^{-1} region. Polarized spectra of a single crystal were measured with a Biorad 575C FT-IR spectrometer using fixed angle specular reflectance accessory. Raman spectra were recorded in both 180° as well as 90° scattering geometry with a Bruker FT-Raman RFS 100/S spectrometer. Excitation was performed with a 1064 nm line of a YAG:Nd^{3+} laser. Blackman-Harris four-term apodization was applied and the number of collected scans was 64. The IR and Raman spectra were recorded with a spectral resolution of 2 cm^{-1}.

The electron absorption spectra were measured at room temperature with a Cary 5 spectrometer.

The emission experiments were performed by using a dye laser with 467 nm as an excitation source and detected with a cooled R 5108 photomultiplier ($\lambda = 400-1200$ nm). The low temperature measurements (10 K) were performed using a Leybold temperature-controlled cryostat.

Diffraction data were obtained with a KUMA-Diffraction KM4CCD four-circle κ-diffractometer equipped with an ultra-low noise CCD detector of 1024×1024 in 2×2 pixels binning. Graphite-monochromated Mo$K\alpha$ X-rays with $\lambda = 0.71073$ Å were generated at 50 kV and 25 mA. A standard data collection was performed at room temperature. The full set of X-ray diffraction data, 1056 frames, was collected over the range 5.5–112° in 2θ in 12 runs with $\Delta\omega = 0.5°$ and $t = 25$ s per frame. The *CrysAlis* software package, ver. 1.171.10 beta (Oxford Diffraction, 2003) [5], were used for data collection (*CrysAlis CCD*) and data reduction, i.e., to transform the CCD frames into integrated intensities (*CrysAlis RED*). The crystal structure was solved and refined using the SHELXS97 and SHELXL97 software [6], respectively.

3. Results and discussion

3.1. Crystal structure

The crystal structure was previously solved for La_3BWO_9 and Eu_3BWO_9 [2]. It was stated that La_3BWO_9 crystallizes in the $P6_3$ and Eu_3BWO_9 in the $P3$ structure. According to Gokhman et al. the $P3$ structure is also adopted by Nd, Sm, Gd, Tb, Dy and Ho borotungstates. The multiplicity in the Bravais primitive unit cells for these structures is equal to $Z = 2$. As a result $2BO_3^{3-}$ ions and $2WO_6$ groups on C_3 sites, as well as $6Ln^{3+}$ ions on C_1 sites are distributed on two distinct crystallographic families in the $P3$ structure. However, our vibrational and luminescence results for these crystals are clearly in contradiction with the established $P3$ structure since they show the presence of only single sites occupied by BO_3^{3-}, WO_6 and Ln^{3+} ions (see discussion in the next paragraphs). We decided, therefore, to reinvestigate the crystal structure of the Eu_3BWO_9 crystals.

The preliminary X-ray studies made on highly twinned sample gave no satisfactory results of the refinement with $P3$ space group (No. 143). The careful choice of the very small sample allowed us to obtain the more reliable diffraction data collected up to $2\Theta = 113.06°$. The sample used in final studies was merohedrally twinned with the second twin component was found to be turned by 60°. The refinement showed that 25.5% of the sample volume corresponds to the

second twin. The analysis of the systematic extinctions shows that the $0\,0\,l$ Bragg reflections are observed up to $l = 12$ for $l = 2n$, only, what clearly indicate $P6_3$ symmetry instead of $P3$. The subsequent analysis by XPREP software strongly confirmed the above result. Therefore, the structure solution and refinement were performed in hexagonal $P6_3$ space group (No. 173). Crystal data, data collection and final refinement parameters are summarized in Table 1. Final atomic parameters and anisotropic displacement parameters are presented in Tables 2 and 3, respectively. Supplementary data for this paper are available in CIF format from the authors. Despite the good reliability factor ($R_1 = 4.53\%$), the residual electron density is higher than expected, and it is placed close to europium atoms at the distances of 0.04 and 0.32 Å for the highest difference peak and the deepest hole, respectively. This is due to the presence of heavy atoms in the structure and to the merohedral twinning. The presence of a twin domain gives rise to the inadequate numerical absorption correction (note the great absorption coefficient).

The crystal structure consists of a set of WO_6 bipyramides stacked along the hexagonal axis and a set of BO_3 triangles (see Fig. 1). The WO_6 bipyramide is formed by two oxygen triangles with slightly different distances from the central W atom (W–O1 and W–O2 distances are 1.966 Å and 1.862 Å, respectively). The triangle formed from the O2 oxygen atoms is rotated by 31.10° with respect to the O1 triangle. It is worth noting that the O1 triangle has nearly the same position for the La_3BWO_9 whereas the O1 triangle in this crystal is rotated by only 3°. Moreover, the anisotropic displacements for the O1 oxygen atoms are larger than the respective values for the O2 atoms. The BO_3 triangles (B–O3 distance of 1.370 Å and B atoms in the plane of oxygen triangle) are rotated with respect to the a-axis by 15.68°.

Table 1
Crystal data and structure refinement for Eu_3BWO_9

Formula weight	794.54
Temperature	298 K
Wavelength	0.71073 Å
Crystal system, space group	Hexagonal, $P6_3$
Unit cell dimensions	$a = 8.5860(10)$ Å $\alpha = 90°$ $b = 8.5860(10)$ Å $\beta = 90°$ $c = 5.4290(10)$ Å $\gamma = 120°$
Volume	346.60(9) Å^3
Z, Calculated density	2, 7.613 mg/m^3
Absorption coefficient	43.334 mm^{-1}
$F(000)$	680
Crystal size	$0.10 \times 0.08 \times 0.07$ mm^3
Theta range for data collection	2.74–56.03 deg.
Limiting indices	$-18 \leqslant h \leqslant 20, -15 \leqslant k \leqslant 19, -6 \leqslant l \leqslant 12$
Reflections collected/unique	9441/2046 [R(int) = 0.0559]
Completeness to theta = 55.50	100.0%
Absorption correction	Numerical
Max. and min. transmission	0.178 and 0.050
Refinement method	Full-matrix least-squares on F^2
Data/restraints/parameters	2046/0/44
Goodness-of-fit on F^2	1.037
Final R indices [$I > 2\sigma(I)$]	$R_1 = 0.0453$, w$R_2 = 0.1234$
R indices (all data)	$R_1 = 0.0486$, w$R_2 = 0.1264$
Absolute structure parameter	0.08(4)
Extinction coefficient	0.0077(9)
Largest diff. peak and hole	9.517 and −13.329 e Å^{-3}

Table 2
Atomic coordinates ($\times 10^4$) and equivalent isotropic displacement parameters (Å$^2 \times 10^3$) for Eu_3BWO_9

	x	y	z	U(eq)
W	6667	3333	7500	5(1)
Eu	6415(1)	7245(1)	7102(2)	6(1)
O(1)	6196(11)	4831(11)	9776(17)	7(1)
O(2)	7277(14)	5278(13)	5417(19)	10(1)
O(3)	1784(11)	1288(11)	8613(17)	7(1)
B	0	0	8670(30)	3(2)

U(eq) is defined as one third of the trace of the orthogonalized U_{ij} tensor.

Table 3
Anisotropic displacement parameters (Å$^2 \times 10^3$) for Eu_3BWO_9

	U_{11}	U_{22}	U_{33}	U_{23}	U_{13}	U_{12}
W	4(1)	4(1)	5(1)	0	0	2(1)
Eu	6(1)	5(1)	6(1)	0(1)	0(1)	3(1)
O(1)	5(2)	6(2)	8(3)	0(2)	0(2)	3(2)
O(2)	11(3)	8(3)	11(3)	5(3)	8(3)	6(3)
O(3)	6(2)	7(3)	8(3)	−2(2)	−3(2)	3(2)
B	4(3)	4(3)	2(5)	0	0	2(2)

The anisotropic displacement factor exponent takes the form: $-2\pi^2[h^2a*^2\,U_{11} + \cdots + 2hka*b*\,U_{12}]$.

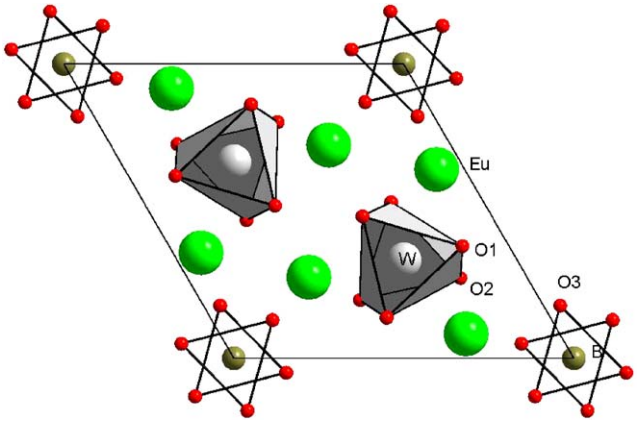

Fig. 1. View of the Eu_3BWO_9 crystal structure.

3.2. Selection rules and vibrational modes

The factor group analysis predicts that there should be $14A + 14B + 14E_1 + 14E_2$ vibrational unit cell modes (see Table 4). Since B–O and W–O bonds are much

Table 4
Factor group analysis for $P6_3$ structure of borotungstate

C_6 symmetry	$n(N)$	$n(T)$	$n(T')$	$n(L(BO_3))$	$n(L(WO_6))$	$n(i(BO_3))$	$n(i(WO_6))$	IR	RS
A	14	1	4	1	1	2	5	z	$xx+yy, zz$
B	14		5	1	1	2	5	—	—
E_1	14	1	4	1	1	2	5	x, y	xz, yz
E_2	14		5	1	1	2	5	—	$xx-yy, xy$

$n(N)$—overall degrees of freedom, $n(T)$—acoustic modes, $n(T')$—translatory lattice modes, $n(L)$—libratory lattice modes, $n(i)$—internal vibrations.

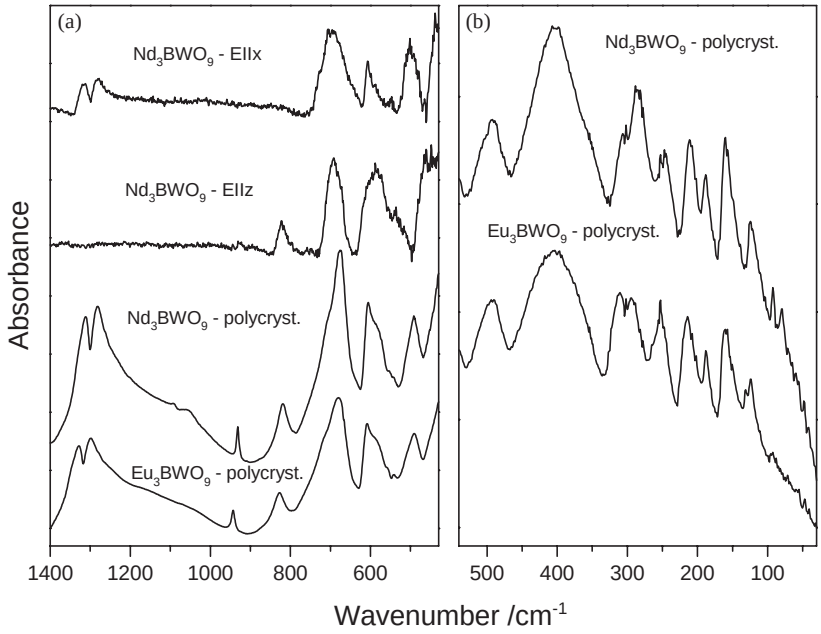

Fig. 2. Polycrystalline (polycryst.) and polarized ($E\|x$ and $E\|z$) IR spectra of Nd_3BWO_9 and Eu_3BWO_9 in the mid-IR (a) and far-IR (b) regions.

stronger than the Eu–O or Nd–O bonds, the structure can be considered as built of BO_3^{3-} and WO_6 molecular groups situated at sites of C_3 symmetry (see Fig. 1). The vibrational modes can be, therefore, subdivided into $3A+3B+3E_1+3E_2$ translational motions of Ln^{3+} ions, $A+B+E_1+E_2$ translational motions of WO_6 polyhedra, $5A+5B+5E_1+5E_2$ internal motions of the WO_6 polyhedra, $A+B+E_1+E_2$ librational modes of the WO_6 polyhedra, $2A+2B+2E_1+2E_2$ internal modes of the BO_3^{-3} ions, $A+B+E_1+E_2$ translational motions of the BO_3^{3-} ions and $A+B+E_1+E_2$ librational motions of the BO_3^{3-} ions. It should be noticed, however, that from the $5A+5B+5E_1+5E_2$ translational modes the E_1+A acoustic modes should be subtracted. The B modes are inactive, the E_2 modes are Raman-active only and the remaining modes are both IR and Raman-active.

The planar BO_3^{3-} free ion, having D_{3h} symmetry, should exhibit the presence of $v_1(A_1')$ and $v_3(E')$ stretching modes, and $v_2(A'')$ and $v_4(E')$ bending modes [7]. The A_1' mode is Raman-active, A_2''—IR active and E' modes are both IR- and Raman-active. In the borotungstate all internal modes should be observed both in IR- and Raman spectra. The v_1 and v_2 modes should appear as A-symmetry modes, and v_3 and v_4 should split into E_1+E_2 components. As far as the WO_6 octahedron with O_h symmetry is concerned, there should be 15 internal degrees of freedom distributed among $A_{1g}+E_g+2F_{1u}+F_{2g}+F_{2u}$ irreducible representations [7]. The $v_1(A_{1g})$, $v_2(E_g)$ and $v_3(F_{1u})$ modes describe stretching vibrations of oxygen atoms and the $v_4(F_{1u})$, $v_5(F_{2g})$ and $v_6(F_{2u})$ modes result from bending motions of the oxygen atoms [7]. The v_1, v_2 and v_5 modes are Raman-active, the v_3 and v_4 modes are IR-active and v_6 mode is both IR- and Raman inactive. In the borotungstate the v_1 modes should be observed as A-symmetry mode, v_2 mode should split into E_1+E_2 components, and each of the remaining modes should be split into E_1+E_2+A+B components.

The recorded spectra are presented in Figs. 2 and 3. The quality of the Raman spectrum, measured for the neodymium compound, is poor because of a strong

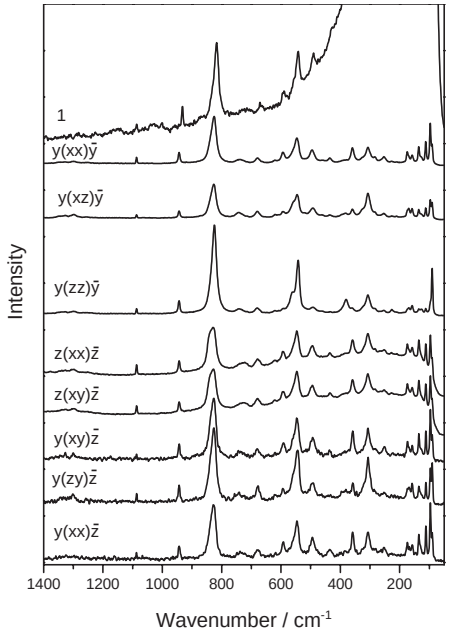

Fig. 3. Raman spectrum of Nd_3BWO_9 in $z(xx+yy+xy)\bar{z}$ configuration (1) and polarized Raman spectra of Eu_3BWO_9 (the remaining plots). The strong background in the spectrum (1) is due to luminescence of Nd^{3+} ions.

luminescence in the 400–0 cm^{-1} region. As a result of this luminescence the spectrum could be recorded using a weak laser power only (70 mW).

The former studies of a number of borates showed that ν_1, ν_2, ν_3 and ν_4 modes of the BO_3^{3-} units are observed around 950, 670–800, 1250–1400 and 600 cm^{-1}, respectively [7,9,10]. The ν_1 symmetric stretching mode is usually observed as the strongest Raman band but its intensity is very low in IR spectra. The opposite behavior is observed for the ν_3 antisymmetric stretching mode and ν_2 out-of-plane bending mode. The ν_4 in plane bending modes are usually observed as weak Raman bands and medium intensity IR bands [7,11]. We may, therefore, unambiguously assign the bands around 1300 (E_1+E_2), 940 (A), 680 (A) and 608–620 (E_1+E_2) cm^{-1} (see Figs. 2 and 3, and Table 5) to the ν_3, ν_1, ν_2 and ν_4 modes, respectively. It can be noticed that there is only one narrow band corresponding to the ν_1 mode of the borate group. This result clearly shows that there is only one distinct BO_3^{3-} ion in the borotungstate structure. This means that the previously established $P3$ structure is not correct since there should be two BO_3^{3-} groups in this case and, therefore, one would expect to observe doublets corresponding to $\nu_1(BO_3)$ mode. The two sharp lines corresponding to the respective modes of the BO_3^{3-} ion were indeed observed for other boron compounds containing two non-equivalent ions, for example, for $Ca_4GdO(BO_3)_3$ [10,11]. The observation of a single $\nu_1(BO_3)$ band is consistent with the $P6_3$ structure.

The ν_1 mode of the WO_6 octahedron can be unambiguously located around 824 cm^{-1} since this mode should have A symmetry, in agreement with our studies, and is always observed as the strongest Raman line around 800–850 cm^{-1} for tungstates [11]. The lack of any noticeable splitting for this mode indicates that there is only one distinct WO_6 octahedron in the crystal structure. This result is another indication that the $P3$ structure is not correct and that the vibrational properties can be better explained when $P6_3$ structure is assumed. The location of the $\nu_2(WO_6)$ mode is less clear since this mode is frequently not observed in the IR and Raman spectra or give rise to very weak Raman band in a very broad wavenumber range, i.e., 500–770 cm^{-1} [12–14]. We suppose that in the studied compounds this mode is observed as weak bands around 720–740 cm^{-1}. The remaining stretching mode of the WO_6 octahedron (ν_3) is always observed as the strongest IR band in the 550–700 cm^{-1} [12,15]. Since in our case the octahedron is strongly distorted, we may expect to observe a significant splitting of this mode into A, E_1 and E_2 components. We assign, therefore, the two strong IR bands around 710 (E_1) and 590 (A) to the two IR-active components of the $\nu_3(WO_6)$ mode. The ν_5 and ν_4 bending modes are usually observed in perovskites as strong Raman bands in the 400–500 cm^{-1} region and strong IR bands in the 300–400 cm^{-1} region, respectively [12,14,15]. In the case of borotungstates these modes are located at slightly higher wavenumbers, i.e., 540–560 and 390–440 cm^{-1}, respectively. The ν_6 bending mode, which is inactive for a regular octahedron, is difficult to locate. We suppose that this mode gives rise to bands in the 280–400 cm^{-1} region.

The lattice modes of the studied crystals are observed below 500 cm^{-1}. According to the previous study of $NdFe_3(BO_3)_4$ the translational motions of the BO_3^{3-} ions are observed around 300–480 cm^{-1}, librational modes of the BO_3^{3-} ions around 150–250 cm^{-1} and translations of the Nd^{3+} ions below 120 cm^{-1} [8]. The studies of a number of perovskites showed, on the other hand, that librational and translational motions of the WO_6 octahedra are located below 200 cm^{-1} [12]. We may, therefore, assign the bands around 490 cm^{-1} and the bands in the 280–390 cm^{-1} region to $T'(BO_3)$ modes. The bands below 270 cm^{-1} can be most likely assigned to coupled modes involving librational motions of the WO_6 octahedra and translational motions of the BO_3^{3-} and Ln^{3+} ions.

The comparison of the spectra recorded for Eu_3BWO_9 and Nd_3BWO_9 crystals shows that the substitution of Nd by Eu results in very minor wavenumber shifts for majority of modes. Clear shifts are, however, observed for $\nu_3(BO_3)$, $\nu_1(BO_3)$ and $\nu_1(WO_6)$ modes indicating shortening of the B–O and W–O distances when Nd is replaced by Eu.

Table 5
Energy of Raman and IR modes in cm^{-1} for Eu_3BWO_9 and Nd_3BWO_9 crystals

Eu_3BWO_9						Nd_3BWO_9		Symmetry	Assignment
Raman $y(xz)\bar{y}$	$y(zz)\bar{y}$	$z(xx)\bar{z}$	$y(xy)\bar{z}$	$y(zy)\bar{z}$	IR	Raman $z(xx+yy+xy)\bar{z}$	IR		
1347vw	1347vw	—	—	—				E_1	$\nu_3(BO_3)$
1327w	1329vw	1330vw	1334w	1335w	1328s	1310w	1312s	E_1	$\nu_3(BO_3)$
1299w	1298vw	1300vw	1298w	1301w	1298s	1283w	1282s	E_2	$\nu_3(BO_3)$
943w	943w	943m	943w	943w	943w	932w	931w	A	$\nu_1(BO_3)$
825m	824s	827s	827s	825s	827m	818s	818m	A	$\nu_1(WO_6)$
743w	741w	?	738w	742w	—	731w	—	E_1+E_2	$\nu_2(WO_6)$
—	—	726w	—	—	—	719w	—	E_2	$\nu_3(WO_6)$
715vw	714vw	—	—	—	711sh	—	712sh	E_1	$\nu_3(WO_6)$
680w	680w	679w	679w	677w	680s	670w	676s	A	$\nu_2(BO_3)$
619vw	620w	620w	—	619vw	—	615vw	—	E_2	$\nu_4(BO_3)$
608vw	609vw	—	—	—	608m		606m	E_1	$\nu_4(BO_3)$
592w	591vw	593m	592m	593w	588s	588vw	584s	A	$\nu_3(WO_6)$
555sh	560sh	554sh	556sh	556sh	557sh	559sh	554vw	E_1+E_2	$\nu_5(WO_6)$
546m	542s	545s	547s	544s	541w	541s	544vw	A	$\nu_5(WO_6)$
493w	492w	493m	493m	493m	492m	487w	491m	E_1+E_2	$T'(BO_3)$
462vw	462vw		—	—	—	—	—		
435vw	434vw	435w	437w	—	—	429w	—	E_2	$\nu_4(WO_6)$
392sh			—	395w	405s	—	402s	E_1+A	$\nu_4(WO_6)$
382w	380m	380vw	—	381w	—	378w	—	A	
359w	361vw	358m	358m	357m	—		—	E_2	
322sh	321sh	317sh		316sh	—		—		$T'(BO_3)$ and
306m	307m	307s	307m	306s	311m		304w	E_1	$\nu_6(WO_6)$
285sh	284vw	283w	—	—	294m		285m		
		266vw	—	—	260sh		—		
253vw	253w	252w	252w	253w	253m		249w	E_1	
227vw	226w	227vw	—	—	—		—	A	
211vw	212vw	210vw	—	—	214m		210m	E_1	
173sh	173sh	174m	173m	—	188w		188w	E_1	$L(BO_3)$, $L(WO_6)$
169vw	169w	170sh		168w	—		—	E_2	$T'(WO_6)$ and
158w	158w	158m	157w	157m	160m		160m	A	$T'(Ln^{3+})$
135w	135w	135m	135m	135m	131vw		—	E_2	
129sh	127w	128sh	129sh	129sh	123w		124w	A	
112w	112w	112m	111m	111w	—		—	E_2	
97m	95sh	96m	96s	97s	94vw		92vw	A	
91m	90s	91sh	90w	90s	—		80vw	A	

s, sh, m, w and vw denote strong, shoulder, medium, weak and very weak, respectively.

Since the crystal structure is non-centrosymmetric, the A and E_1 modes are both IR and Raman active. The macroscopic electric field associated with these modes should, therefore, modify their wavenumbers. If $q\|z$, there are only degenerate pairs of purely transverse (TO) modes of E_1 symmetry and purely longitudinal (LO) modes of A symmetry. If $q\|y$ the degeneracy of the E_1 modes is lifted (TO–LO splitting) whereas the A modes are necessarily of the TO type. The performed measurements show that for majority of modes the wavenumbers of vibrational modes are nearly the same, irrespective on the phonon propagation direction. However, in case of the doubly degenerated $\nu_3(BO_3)$ mode we observe that the single band at $1330\,cm^{-1}$ when $q\|z$ shifts towards $1335\,cm^{-1}$ when q forms 45° angle with z-axis and is clearly split into two components for $q\|y$ (see Table 5 and Fig. 3). This splitting can be most likely attributed to the LO ($1347\,cm^{-1}$)–TO ($1330\,cm^{-1}$) splitting. Another mode showing clearly the q-dependence of wavenumber is the $\nu_1(WO_6)$ mode. This mode appears at $824\,cm^{-1}$ for $q\|y$ (TO mode) and $827\,cm^{-1}$ for $q\|z$ (LO mode). The observation of some weak LO–TO splitting for two modes only indicates that macroscopic electric field and direction dispersion is weak for this class of crystals. Similar weak LO–TO splitting was observed previously for $Pr_xY_{1-x}Al_3(BO_3)_4$ borate [9].

3.3. Electron absorption and luminescence spectra

The electron absorption and luminescence spectra of Eu_3BWO_9 crystal are shown in Figs. 4 and 5 (the

electron absorption and luminescence studies of Nd_3BWO_9 will be presented in a separate paper). Table 6 lists energies of all observed electronic transitions.

The presence of the $^5D_0 \rightarrow {}^7F_{0,3}$ transitions and the J-degeneracy splitting indicate that the Eu^{3+} ions occupy a very low-symmetry sites. The presence of only one $^5D_0 \rightarrow {}^7F_0$ and $^7F_0 \rightarrow {}^5D_0$ transitions clearly shows that only one site is occupied by the Eu^{3+} ion. This result confirms our conclusion derived on the basis of vibrational spectra that the $P3$ structure established previously is incorrect. The presence of only one low-symmetry site is, however, consistent with the $P6_3$ structure.

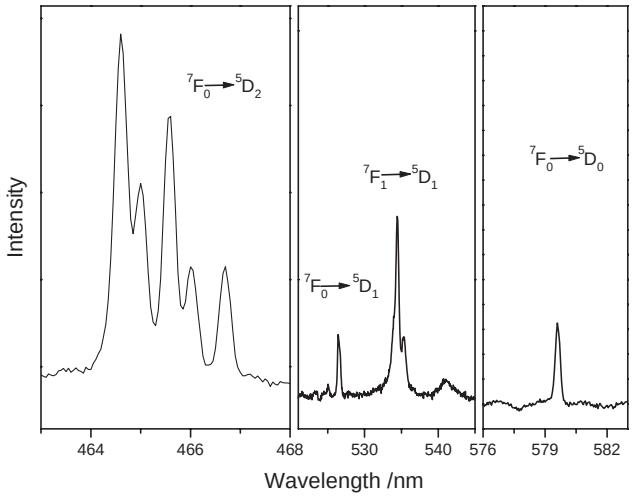

Fig. 4. Room-temperature electron absorption spectrum of Eu_3BWO_9 corresponding to $^7F_0 \rightarrow {}^5D_{0-2}$ and $^7F_1 \rightarrow {}^5D_1$ transitions.

It is well known that luminescence studies of Eu^{3+} may give insight on the nature of the cation surrounding [16–21]. First of all, the intensity of the $^5D_0 \rightarrow {}^7F_0$ transition can be explained by J-mixing effects involving $^7F_0$ and $^7F_2$ levels [16,17]. Our studies show that the ratio between the integrated intensity of the $^5D_0 \rightarrow {}^7F_0$ and $^5D_0 \rightarrow {}^7F_2$ emission transitions is 0.052. This ratio is significantly higher than that observed for Eu^{3+} ions in xerogels [17], indicating significant J-mixing effects. Secondly, it has been shown that the red shift in the $^5D_0 \rightarrow {}^7F_0$ energy from the 17374 cm^{-1} value calculated for gaseous Eu^{3+} increases with increasing Eu^{3+}-ligand covalency [17,18]. This red shift, $-122\,cm^{-1}$ for the Eu_3BWO_9, is of similar value as that found for other materials with oxygen ligands, for example, complex of urea or poly(oxyethylene) with $EuBr_3$ [17]. This result indicates a similar Eu^{3+}-oxygen covalency in these compounds and Eu_3BWO_9. Thirdly, it is worth noting that covalency also strongly influences intensity of the $^5D_0 \rightarrow {}^7F_1$ transition [16,17,19–21]. The ratio between $^5D_0 \rightarrow {}^7F_2$ and $^5D_0 \rightarrow {}^7F_1$ transitions increases with increasing covalency [16,17,19]. However, this ratio increases also with increasing polarization and distortion of the Eu^{3+} environment [16,17,19–21]. In the case of Eu_3BWO_9 this ratio is 19.3. This value is significantly higher than the value obtained for a complex of urea with $EuBr_3$ (4.22 [17]), in spite of the fact that similar Eu^{3+}-oxygen covalency is predicted for the both compounds (see discussion above). We may conclude, therefore, that the large I_{0-2}/I_{0-1} ratio for Eu_3BWO_9 indicates strong distortion of the Eu^{3+} environment. This conclusion is consistent with the established $P6_3$ structure.

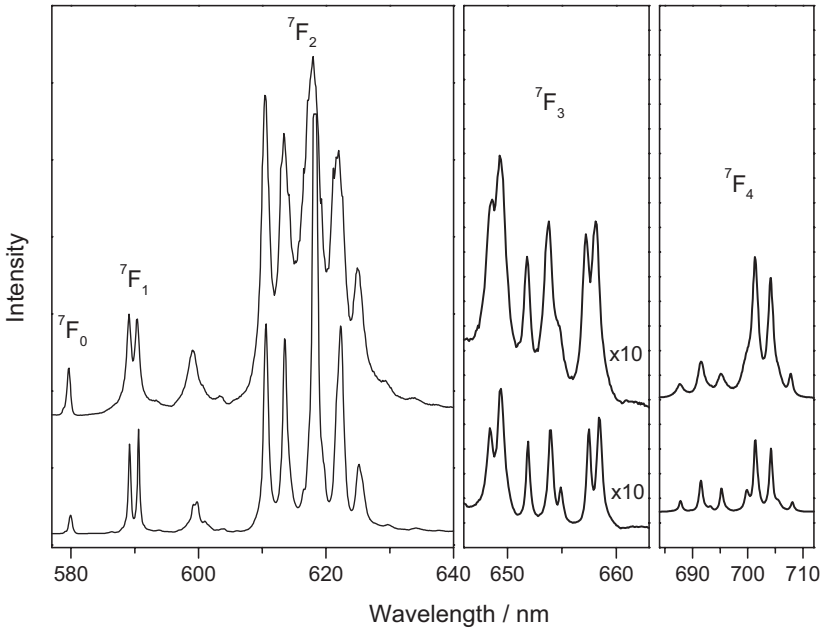

Fig. 5. Luminescence spectra at room (upper trace) and 10 K (lower trace) temperature of Eu_3BWO_9 corresponding to the $^5D_0 \rightarrow {}^7F_{0-4}$ transitions.

Table 6
Absorption and emission peaks (in cm^{-1}) of Eu^{3+} in Eu_3BWO_9 together with assignment

Transition	Energy	Number of components	
		Theoretical	Observed
Emission			
$^5D_0 \rightarrow {}^7F_0$	17252	1	1
$^5D_0 \rightarrow {}^7F_1$	16937, 16975	3	2
$^5D_0 \rightarrow {}^7F_2$	15995, 16080, 16187, 16301, 16382	5	5
$^5D_0 \rightarrow {}^7F_3$	15195, 15217, 15273, 15296, 15342, 15397, 15418	7	7
$^5D_0 \rightarrow {}^7F_4$	14128, 14173, 14201, 14258, 14291, 14384, 14434, 14461, 14541	9	9
Absorption			
$^7F_0 \rightarrow {}^5D_0$	17253	1	1
$^7F_1 \rightarrow {}^5D_1$	18678, 18710, 18724	3	3
$^7F_0 \rightarrow {}^5D_1$	18993, 19004, 19046	3	3
$^7F_0 \rightarrow {}^5D_2$	21427, 21390, 21478, 21506, 21525	5	5

4. Conclusions

The IR, Raman, X-ray, electron absorption and luminescence studies confirm the non-centrosymmetric structure of the Nd- and Eu-borotungstates and show that the unit cell of Eu_3BWO_9 contains only one non-equivalent BO_3^{3-} and lanthanide ion, and one WO_6 unit. These results show that the previously reported Eu_3BWO_9 crystal structure of $P3$ symmetry is not correct. The crystal structure is of $P6_3$ symmetry, i.e., the same as that found for the La compound. This symmetry explains also well the vibrational and electronic properties of this compound. The similarity of the IR and Raman spectra recorded for the Eu- and Nd-borotungstates allows us to suppose that the structure of Nd_3BWO_9 can be also described by the $P6_3$ symmetry.

Acknowledgments

We would like to thank Prof. A. Pietraszko for X-ray measurements.

References

[1] S.Yu. Stefanovich, N.U. Venskovskii, A.V. Mosunov, V.A. Krut'ko, Russ. J. Inorg. Chem. 46 (2001) 1864.
[2] L.Z. Gokhman, B.F. Dzhurinskii, V.A. Efremov, A.B. Ilyukhin, V.I. Chistova, Russ. J. Inorg. Chem. 39 (1994) 1026.
[3] B.F. Dzhurinskii, G.V. Lysanova, Russ. J. Inorg. Chem. 43 (1998) 1931.
[4] A. Majchrowski, E. Michalski, A. Brenier, J. Cryst. Growth 247 (2003) 467.
[5] Oxford Diffraction, CrysAlis Data Reduction Software (version 1.171.10 beta), Oxford Diffraction, Wrocław, Poland, 2003.
[6] G.M. Sheldrick, SHELXS97 and SHELXL97, University of Göttingen, Germany, 1997.
[7] K. Nakamoto, Infrared and Raman Spectra of Inorganic and Coordination Compounds, Wiley, New York, 1986.
[8] A. de Andrés, F. Agulló-Rueda, S. Taboada, C. Cascales, J. Campá, G. Ruiz-Valero, I. Rasines, J. Alloys Compd. 250 (1997) 396.
[9] H.R. Xia, L.X. Li, J.Y. Wang, W.T. Yu, P. Yang, J. Raman Spectrosc. 30 (1999) 557.
[10] A. Lorriaux-Rubbens, G. Aka, E. Antic-Findancev, D.A. Keszler, F. Wallart, J. Raman Spectrosc. 31 (2000) 535.
[11] G. Dominiak-Dzik, W. Ryba-Romanowski, S. Gołąb, L. Macalik, J. Hanuza, A. Pajączkowska, J. Mol. Struct. 555 (2000) 213.
[12] M. Liegeois-Duyckaerts, P. Tarte, Spectrochim. Acta A 30 (1974) 1771.
[13] I. Gregora, J. Petzelt, J. Pokorný, V. Vorliček, Z. Zikmund, R. Zurmühlen, N. Setter, Solid State Commun. 94 (1995) 899.
[14] R. Tao, A.R. Guo, C.-S. Tu, I. Siny, R.S. Katiyar, Ferroelectrics Lett. 21 (1996) 79.
[15] J. Petzelt, E. Buixaderas, A.V. Pronin, Mater. Sci. Eng. B 55 (1998) 86.
[16] O.L. Malta, M.A. Counto dos Santos, L.C. Thompson, N.K. Ito, J. Lumin. 69 (1996) 77.
[17] L.D. Carlos, R.A. Sá Ferreira, V. De Zea Bermudez, C. Molina, L.A. Bueno, S.J.L. Ribeiro, Phys. Rev. B 60 (1999) 10042.
[18] S.T. Frey, W. De, W. Horrocks, Inorg. Chim. Acta 229 (1995) 383.
[19] E.W.J.L. Oomen, A.M.A. van Dongen, J. Non-Cryst. Solids 111 (1989) 205.
[20] V. Di Noto, M. Bettinelli, M. Furlani, S. Lavina, M. Vidali, Macromol. Chem. Phys. 197 (1996) 257.
[21] A. Ferry, M. Furlani, A. Franke, P. Jacobsson, B.-E. Mellander, J. Chem. Phys. 109 (1998) 2921.